Glucagon Amyloid-like Fibril Morphology Is Selected via Morphology-Dependent Growth Inhibition†

Christian Beyschau Andersen,‡,§ Daniel Otzen,§ Gunna Christiansen,|| and Christian Rischel*,‡

Protein Structure and Biophysics, Novo Nordisk A/S, Novo Nordisk Park, DK-2760 Måløv, Denmark, Centre for Insoluble Protein Structures (inSPIN), Department of Life Sciences, Aalborg University, Sohngaardsholmsvej 49, DK-9000 Aalborg, Denmark, and Institute of Medical Microbiology and Immunology, University of Aarhus, Wilhelm Meyers Allé, DK-8000 Århus C, Denmark

Received December 11, 2006; Revised Manuscript Received April 19, 2007

ABSTRACT: The 29-residue peptide hormone glucagon readily fibrillates at low pH, but the structure and morphology of the fibrils are very sensitive to the environmental conditions. Here we have investigated the mechanism behind the differences in morphology observed when glucagon fibrils are formed at different peptide concentrations. Electron microscopy shows that fibrils formed at low glucagon concentration (0.25 mg/mL) are twisted, while fibrils formed at high concentration (8 mg/mL) are straight. Monitoring the fibrillation kinetics at different concentrations, we find that the lag time has an unexpected maximum at a concentration of 1 mg/mL, with faster fibrillation at both lower and higher concentrations. Seeding experiments show that small amounts of straight fibril seeds can accelerate fibril growth at both low and high glucagon concentration, while twisted fibril seeds cannot grow at high concentrations. We conclude that there exists a morphology-dependent mechanism for inhibition of glucagon fibril growth. Light scattering experiments indicate that glucagon is mainly monomeric below 1 mg/mL and increasingly trimeric above this concentration. We propose that the glucagon trimer is able to specifically inhibit growth of the twisted fibril morphology. Such inhibitory binding of molecules in an unproductive conformation could also play a role in the selection of morphologies for other fibril-forming peptides and proteins.

Most if not all proteins are able to form extended, insoluble structures known as fibrils (*1*). In the form of fibrils or even fibril precursors, the protein may not only be unable to perform its biological function but even be harmful to organisms. This is seen in conditions such as Alzheimer's disease, Parkinson's disease, and prion diseases. The ease by which many proteins form fibrils in vitro also poses a great challenge to protein production and formulation in the pharmaceutical industry (*2*). The morphology of fibrils is typically very diverse (*3*) and under influence of the conditions in which fibrillogenesis takes place, but the mechanisms behind the preference for particular morphologies are largely unknown.

The 29 amino acid polypeptide glucagon is a hormone involved in the regulation of blood sugar levels. It readily forms polymorphic fibrils, which have been studied by various biophysical methods including atomic force microscopy (AFM),[1] transmission electron microscopy (TEM), fluorescence, and circular dichroism (CD) (*3*−*6*). The aim of the work presented here is to study the origin of fibril polymorphism, specifically the influence of the protein concentration.

MATERIALS AND METHODS

Buffer and Peptide Solutions. The buffer solution was prepared by dissolving glycine in Milli-Q water and adjusting the pH to 2.5 by adding 4.0 M HCl. The buffer was filtrated through a 0.22 μm sterile cellulose acetate filter. Freeze-dried glucagon (Novo Nordisk A/S) was dissolved in buffer by gentle shaking and left to stand for a few minutes before use. Peptide concentrations were determined by measuring the absorbance on a spectrophotometer (Ultrospec 4000; Pharmacia Biotech) and using a theoretical molar extinction coefficient of $\epsilon_{280} = 8250\ M^{-1}\ cm^{-1}$. A thioflavin T stock solution was prepared by dissolving 2 mM ThT in Milli-Q water. The stock solution was kept at 5 °C where it remains stable for several months.

Fibrillation Kinetics. Fibrillation kinetics was followed by adding ThT to the glucagon solution to a final concentration of 40 μM and measuring the fluorescence intensity of ThT. The experiments were performed at 25 °C using 96-well plates (catalog no. 7706−2370, Corning Inc.) sealed with tape pads in a fluorescence plate reader (SpectraMax Gemini EM; Molecular Devices) programmed to read every 10 min at an excitation wavelength of 444 nm and an emission wavelength of 488 nm. The samples were not shaken except for the motion of the plate during reading. Fluorescence from tryptophan residue 25 of glucagon was read with excitation

† C.B.A. benefits from a Ph.D. scholarship cofinanced by Novo Nordisk A/S and the Danish Ministry of Science, Technology, and Innovation.

* Corresponding author. E-mail: cris@novonordisk.com. Tel: +45 3079 0513. Fax: +45 4466 3939.

‡ Novo Nordisk A/S.

§ Aalborg University.

|| University of Aarhus.

[1] Abbreviations: AFM, atomic force microscopy; CD, circular dichroism; DLS, dynamic light scattering; SLS, static light scattering; SVD, singular value decomposition; TEM, transmission electron microscopy; ThT, thioflavin T; Trp-25, tryptophan residue 25.

10.1021/bi6025374 CCC: $37.00
Published on Web 05/25/2007

at 300 nm and emission at 330 and 355 nm. The fluorescence signal undergoes a significant blue shift when the peptide is integrated in fibrils (*3*), thus making the 330/355 nm ratio useful as a probe of the fibrillation kinetics. The signal is, however, much weaker and noisier than the signal from ThT.

Lag Times and Growth Rates. We define the lag time as the time it takes for the ThT signal or Trp fluorescence 330/355 nm ratio to increase from initial levels to 5% of the maximum increase (*7*). As the fibrillation curves of lowest concentrations suffer from a low signal-to-noise ratio, these data were fitted to a sigmoid curve, and the lag time was determined from the fit:

$$y(t) = A + \frac{B}{\left[1 + \exp\left(\frac{-(t - C)}{D}\right)\right]^E}$$

where A represents the initial fluorescence intensity, B the final intensity plateau, C the midpoint of the elongation phase, D the elongation rate, and E a parameter whose magnitude reflects the asymmetry of the sigmoid curve. Growth rates were calculated by making a standard exponential fit to the fibrillation curves from time zero to a point where the background-subtracted fluorescence intensity had reached 25% of the maximum value (*7*). Data analysis was made in Matlab 7.0 (Mathworks). Visually, both sigmoid and exponential functions fitted the data very well.

Electron Microscopy. Glucagon solutions were incubated at 25 °C in the fluorescence plate reader and samples removed at specific points on the fibrillation curve. The samples were diluted 1, 5, or 20 times in buffer and immediately transferred to a 400-mesh carbon-coated, glow-discharged grid for 30 s. Grids were washed in two drops of doubly distilled water, stained with 1% phosphotungstic acid (pH 6.8), and blotted dry on filter paper. Samples were viewed on a transmission electron microscope (JEM-1010; JEOL) operating at 60 kV.

Seeding Experiments. The amount of unfibrillated glucagon was determined by spinning fibrillated samples at 32000*g* for 15 min and measuring the protein concentration in the top fraction. The unfibrillated fibril mass amounted to less than 5% and is hence negligible when calculating the seed concentrations below. Seed stock solutions were prepared by incubating 0.25 and 8 mg/mL glucagon solutions in the fluorescence plate reader at 25 °C. When the ThT fluorescence signal for each solution had reached its maximum, the solutions were transferred to two separate Seed Bead tubes (Hampton Research) designed to crush protein crystals and then vortex mixed thoroughly. From seed stock solutions that were either undiluted or 100 or 10000 times diluted in buffer, aliquots were mixed with fresh solutions of 0.25 and 8 mg/mL glucagon. In both cases, we chose a maximum seed volume at 5% of the monomer solution. Finally, 200 μL portions of the seeded solutions were transferred to 96-well microtiter plates and incubated in the plate reader at 25 °C. The amount of seed in the final mixture is reported as the mass of seeds compared to the volume of fresh glucagon solution. The seed concentrations were in the range from 10^{-3} to 400 μg/mL (seeds formed at 8 mg/mL) and from 3.2×10^{-5} to 12.5 μg/mL (seeds formed at 0.25 mg/mL) with intermediate values separated by a factor of 5. Calculation of lag times and growth rates were made in Matlab 7.0 as described above.

Light Scattering Experiments. Light scattering experiments were performed in 1.5 mm quartz cuvettes using a DynaPro 99 dynamic light scattering instrument (Protein Solutions Inc.). An acquisition time of 5 s was used, and at least 30 acquisitions made up a single measurement. To estimate the molecular weight of glucagon as a function of concentration, we used a method developed by Lindner and Glatter (*8*, *9*), which combines dynamic light scattering (DLS) and SLS. DLS measures diffusion coefficients of molecules in solution and also estimates the fraction of light scattered from each molecular species. In this way, DLS helps to separate light scattering from small oligomers from the signal from dust or minute amounts of large aggregates. The intensity distribution of the diffusion coefficients was determined from the light scattering data using the Dynamics software (version 5.26; Protein Solutions Inc.). This gives the fraction f of the intensity that is due to the monomer/oligomer signal. The average molecular weight is then calculated as (*8*, *9*)

$$M_w = \frac{f(I_{tot} - I_{buf})}{Kc}$$

where I_{tot} is the total scattered intensity, I_{buf} is the intensity from a buffer sample, c is the glucagon concentration in milligrams per milliliter, and K is a calibration constant. Reproducibility was checked by repeating the measurements on a given solution in three different cuvettes. In measurements on reference proteins on our setup, the calibration constant K typically varies by $\pm$10%. For the present case, we chose the value within this interval that has glucagon monomeric at low concentration. The molecular weight is reported in terms of the oligomer size.

Circular Dichroism Spectroscopy. CD spectra of freshly dissolved glucagon were recorded on a spectropolarimeter (Chirascan; Applied Photophysics) over the wavelength range of 200−260 nm with a step size of 1 nm, a 1 nm bandwidth, and a scan rate of 15 nm/min. The temperature was fixed at 20 °C using the built-in temperature control. Depending on the absorption of the sample, quartz cuvettes of 0.1, 0.2, 0.5, or 1.0 mm path lengths were used. The background was subtracted from each spectrum, but no additional filtering or noise reduction was applied. The raw ellipticity is converted to molar ellipticity through the relation

$$\Delta\epsilon = \theta \frac{0.1 M_w}{l c N_{res} \times 3298}$$

where the following abbreviations are used: θ is the raw ellipticity, M_w is the molecular weight in daltons, l is the length of the light path in centimeters, c is the concentration in milligrams per milliliter, and N_{res} is the number of residues.

Singular Value Decomposition. Spectroscopy data often consist of a set of spectra covering some transition. It is in many cases expected that all spectra in the set are linear superpositions of a few basis spectra representing the underlying states of the transition. If only two states are present and the data are normalized properly, the data set will have a constant value at a point where the basis spectra cross, in the case of CD an isodichroic point. We analyzed our CD data series by the more general method of singular

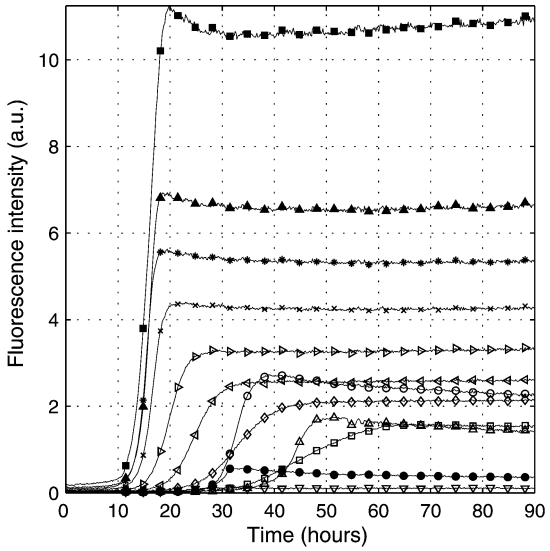

FIGURE 1: Fibrillation of glucagon at various concentrations measured by ThT fluorescence at 488 nm. Key: (■) 8 mg/mL, (▲) 6 mg/mL, (*) 5 mg/mL, (×) 4 mg/mL, (+) 3 mg/mL, (▼) 2.5 mg/mL, (◊) 2 mg/mL, (□) 1.5 mg/mL, (△) 1 mg/mL, (○) 0.75 mg/mL, (●) 0.5 mg/mL, and (▽) 0.25 mg/mL.

value decomposition (SVD). To apply SVD, the experimental data are organized into a matrix with each column representing a spectrum, and the SVD calculation then attempts to reduce the entire set of spectra to superpositions of as few basis vectors as possible. The most important output is the list of singular values, which represents the importance of the calculated basis vectors. Often, the first two or three values are significantly larger than the remaining values, indicating that the experimental data are linear combinations of only two or three independent basis spectra. A more detailed description of the method can be found in ref *10*. Calculations were done using a free add-in to Excel (*11*).

RESULTS

Fibrillation Kinetics. Glucagon fibrils have been shown to interact with the fibril-specific dye ThT, causing the ThT fluorescence at 488 nm to increase upon fibril formation (*3*). In a number of fibrillation experiments, we measured ThT fluorescence in 96-well microtiter plates at 25 °C every 10 min for up to 90 h. The concentrations ranged from 0.25 to 8 mg/mL, and at each concentration data were collected from four replica wells. Representative fibrillation curves are shown in Figure 1. Lag times and growth rates were calculated as detailed in Materials and Methods and plotted as a function of the glucagon concentration in the top and bottom panel of Figure 2. Full symbols show results from one batch of glucagon, where we performed experiments at a large number of concentrations. Open symbols show results from identical experiments on a different batch, where we made two separate repetitions of the experiment. The lag time plot shows a clear maximum in lag times around 1−1.5 mg/mL. This behavior is mirrored by the variation in growth rates. Below 1.5 mg/mL the growth rates decrease with increasing concentration, while above 1.5 mg/mL the growth rates increase with increasing concentration. Although the anomalous maximum in the lag time is present for both batches, there seems to be some batch-to-batch variation.

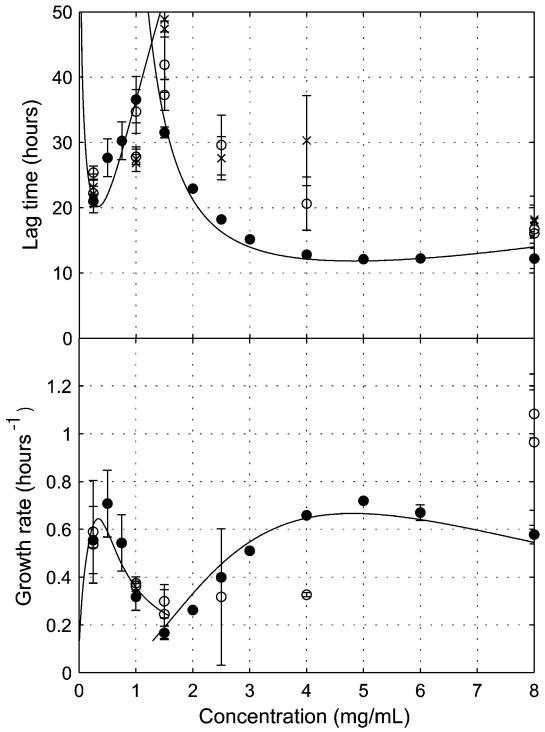

FIGURE 2: Lag times and growth rates of the fibrillation curves shown in Figure 1. Solid and open symbols show the results from two different glucagon batches. Crosses show the results of analyzing the tryptophan 330/355 nm signal from samples without ThT. Error bars represent the standard deviation from fibrillation at identical conditions in four separate wells. The full lines represent fits of the solid symbols to a theoretical model (see Discussion and Appendix for details).

The fibrillation model (see below) was fitted to the solid symbols (full lines).

The intrinsic fluorescence of Trp-25 provides an alternative probe for fibrillation (*3*) although the intensity is low compared to the signal from ThT. In the experiments on the second batch, glucagon solutions at various concentrations were split in two, and ThT was added to one part. In this way, it was possible to compare lag times calculated from ThT and Trp-25 fluorescence curves and examine any effect ThT may have on fibrillation kinetics. The crosses in Figure 2 show lag times calculated from the 330/355 nm intensity ratio in the wells without ThT. They are seen to agree with the lag times from the ThT graphs (open symbols) within experimental error. Calculation of rate constants from the noisy Trp-25 fluorescence data is not reliable.

Morphology. We investigated how changes in fibrillation kinetics were reflected in the overall structure of the formed fibrils. The morphology of glucagon fibrils formed at different concentrations was subjected to analysis by TEM by transferring samples directly from the fluorescence plate reader to the grid. In one set of experiments, each sample was studied immediately after it had reached the maximum fluorescence intensity. The fibrils observed belonged to one of two morphologies. One type of fibrils consisted of two or more filaments twisted around each other with a regular twist. The width of the twisted fibrils was approximately 14 nm. The other type consisted of straight, nontwisted fibrils consisting of just one filament. These straight morphology fibrils were cylindrical with a diameter of approximately 6 nm, but careful inspection revealed a faint periodic pattern.

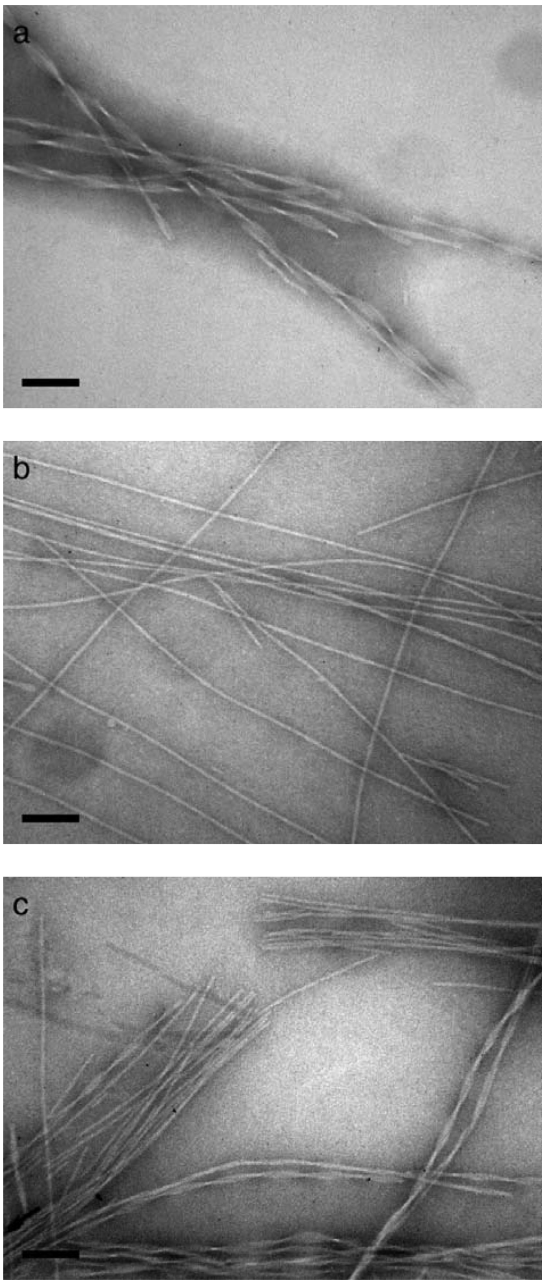

FIGURE 3: TEM pictures of glucagon fibrils formed at three different concentrations reveal a change in morphology. (a) 0.25 mg/mL. At low concentration, the majority of the fibrils consist of two or more filaments twisted around each other. The width of the fibrils is approximately 14 nm and the twist repeat approximately 80 nm. (b) 8 mg/mL. At high concentration, the fibrils are primarily straight, although a very small population of twisted fibrils are present. The width of the straight fibrils is approximately 6 nm. (c) 1.5 mg/mL. At an interval between high and low concentration both straight and twisted morphologies are present. Scale bar represents 100 nm.

This indicates that the single filament is actually made from protofilaments (*12*). The morphologies observed are in line with previous work (*3*). Samples obtained at 0.25−0.5 mg/mL were dominated by the twisted morphology (Figure 3a) with just a small fraction of straight, linear fibrils. Samples obtained at 2.5−8 mg/mL were almost exclusively straight fibrils (Figure 3b), although a small fraction consisted of twisted fibrils and what appeared to be pairwise bundled, untwisted fibrils. In the interval from 0.5 to 2.5 mg/mL both straight and twisted fibril morphologies were found, with twisted fibrils becoming increasingly rare and straight fibrils increasingly numerous as the glucagon concentration increased (Figure 3c).

ThT fluorescence curves from fibrillating 0.5, 0.75, and 1 mg/mL glucagon showed a gradual decrease in fluorescence intensity seen in the late part of the fibrillation curves (Figure 4a). To examine this behavior, low concentration samples (0.5 mg/mL) were examined immediately after the maximum intensity was reached and after 64 h where the intensity had dropped by approximately 30%. At 0.5 mg/mL the maximum fluorescence intensity is reached after 39 h, and TEM showed that regularly twisted fibrils are formed (Figure 4b). After 64 h, the intensity had dropped, and an opaque, dense network of fibrils has formed (Figure 4c). By diluting the sample 10-fold in the same buffer, the dense network dissolves and reveals twisted fibrils visually identical to the fibrils formed after 39 h (Figure 4d). For comparison, a sample at high concentration (8 mg/mL) was subjected to the same analysis. Though no decrease in fluorescence intensity is observed, a similar fibril network was formed. The dense fibril network could also in this case be dissolved by diluting the sample in the same buffer, and once again the straight fibril morphology was shown to be conserved (data not shown). The decrease in fluorescence intensity after the maximum has been reached can in principle shift the lag time compared to the ideal case without decrease. The smooth line in Figure 4a shows a fit of the fluorescence intensity data up to 50 h to the function $I(t) = A + [B + \alpha(t - C)]/[1 + \exp(-(t - C)/D)]^E$, where the sigmoidal form is modified by the slope α. With this function, we obtain a 29.7 h lag time, still defined by $I(t)$ reaching 5% of the maximum intensity. The effect of the decrease in fluorescence can be probed by setting $\alpha = 0$ and keeping the other parameters fixed. The lag time of the resulting curve is 29.8 h. The time determined from the experiment is 30.2 h. These differences are well within the experimental variation.

Seeding Experiments. To investigate how well the different glucagon fibril species act as templates for new fibrils, seeds were produced from samples containing mature fibrils grown at 0.25 and 8 mg/mL, respectively. Fractions of these two seed stocks were added to fresh solutions of 0.25 and 8 mg/mL glucagon. Fibrillation kinetics of the seeded solutions was monitored by ThT fluorescence, and the resulting lag times are plotted in Figure 5. Seeding a fresh 0.25 mg/mL glucagon solution with seeds from fibrils formed at either 0.25 or 8 mg/mL glucagon solution causes a large reduction in lag time (Figure 5a). In the absence of seeds, the lag time is approximately 23 h, but by adding seeds in concentrations higher than 0.1 μg/mL the lag time is strongly reduced. At seed concentrations above 2.5 μg/mL the solution starts to fibrillate immediately. Seeding a fresh 8 mg/mL glucagon solution with seeds of an 8 mg/mL solution also leads to a large reduction in lag time (Figure 5b). The lag time is roughly 13 h without seeds and becomes completely eliminated at maximum seed concentration. However, when seeds, which were formed in a 0.25 mg/mL glucagon solution, were added to a fresh 8 mg/mL glucagon solution, only a modest effect was observed at the highest concentration (Figure 5b).

To determine if the seeding morphology propagated during the seeding experiment, samples seeded with the maximum fraction of seeds were subjected to analysis by TEM (Figure

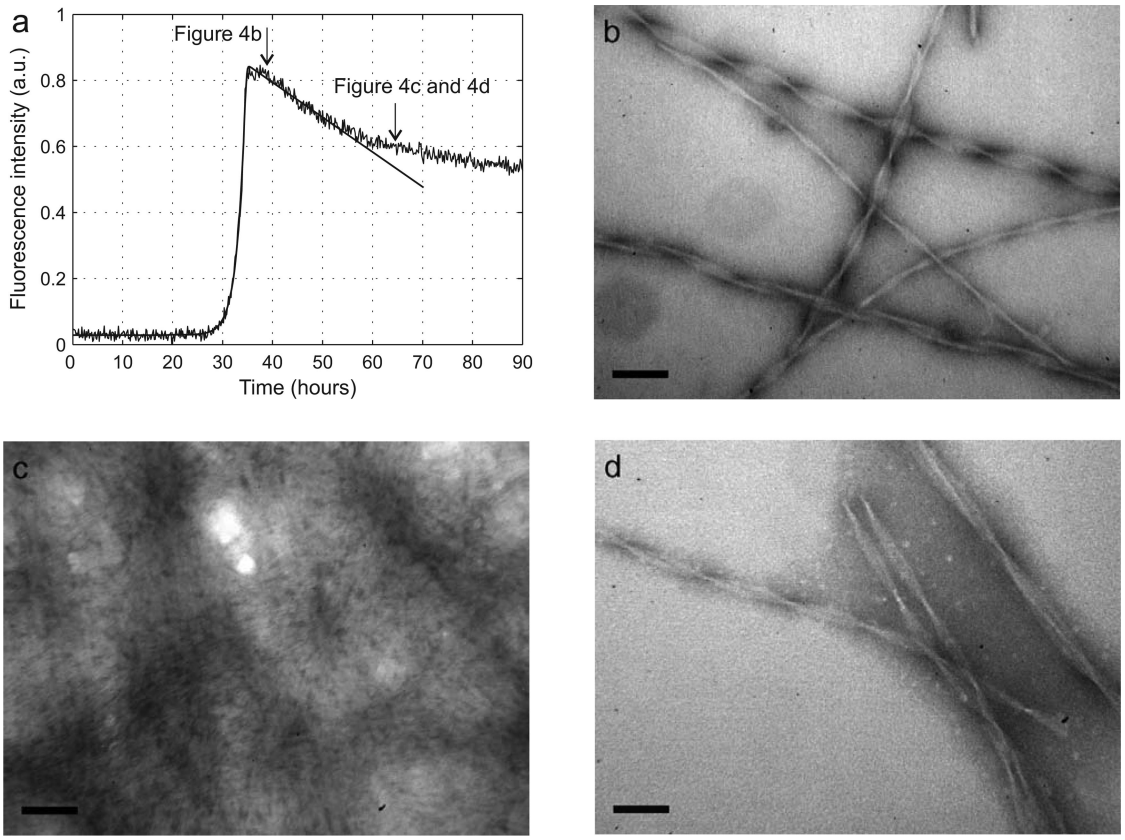

FIGURE 4: Electron microscopy pictures of fibrils formed at 0.5 mg/mL. (a) Trace of the fibrillation curve with arrows indicating the times at which the samples were removed from the well. The full line shows a sigmoidal fit to the data from 0 to 50 h (see main text for details). (b) Picture taken of a nondiluted sample after 39 h. The fibrils are twisted and consist of two or more filaments. (c) After 64 h, the fibrils in the same well have created a dense mesh. The morphology cannot be determined from this nondiluted sample. (d) The same sample as in panel b diluted 10 times. The morphology is twisted as in panel b. Scale bar represents 100 nm.

6). Not surprisingly, TEM revealed that fibrils from a fresh 0.25 mg/mL glucagon solution self-seeded with seeds of a 0.25 mg/mL solution had a twisted morphology (Figure 6a), while the self-seeding experiment of an 8 mg/mL solution with seeds of an 8 mg/mL solution showed fibrils of straight morphology (Figure 6b). Cross-seeding a 0.25 mg/mL solution with seeds of an 8 mg/mL solution showed that the fibrils inherit the (straight) morphology of the 8 mg/mL seeds (Figure 6c). Interestingly, the opposite cross-seeding experiment, where a fresh 8 mg/mL solution was seeded with (twisted) seeds from a 0.25 mg/mL solution, also resulted in straight fibrils (Figure 6d).

Self-Association of Glucagon. We next investigated the oligomerization state of glucagon. Using the Lindner−Glatter light scattering method, the average molecular weight was determined in glucagon solutions with concentrations in the range of approximately 0.16−8 mg/mL (Figure 7). These molecular weights demonstrate that as the concentration is increased, the oligomer size increases from 1 to approximately 2.6. Hence the light scattering data support previous work that demonstrated the existence of a monomer−trimer equilibrium in acidic glucagon solutions (*13*). In a separate experiment, 1 mg/mL glucagon solutions were spiked with Na_2SO_4 and NaCl in order to explore if ions are capable of stabilizing the trimer. The results are plotted as solid symbols in Figure 7.

To further investigate the nature of the species observed by light scattering, CD spectra were recorded in solutions of 0.16−5 mg/mL glucagon (Figure 8a). The data consisting of 11 CD spectra were analyzed by singular value decomposition (SVD). SVD shows (Figure 8b) that the weights of the first two basis spectra, 44.5 and 7.60, are respectively 202 and 35 times higher than the weight of the third most important basis spectrum, 0.22, demonstrating that all of the measured spectra can be obtained by weighted sums of just two basis spectra. Thus, CD data support the results from cross-binding experiments (*13*) that only two species are significantly populated at these glucagon concentrations. SVD also returns a set of orthonormal basis spectra, the first three of which are shown in the inset of Figure 8b. The third basis spectrum shows random fluctuations, confirming the two-state nature of the trimerization process. Each recorded spectrum is essentially a linear combination of the two basis spectra, and the basis spectra by themselves do not necessarily have a physical meaning.

DISCUSSION

Previous work has established the ability of glucagon to form amyloid-like fibrils of different morphology (*14*, *15*) and the promotional effect on fibrillation rates of adding salt, increasing pH, and increasing temperature to 30 °C (*14*). Later work by Pedersen et al. (*3*) took an in-depth look at the conditions leading to different fibril morphologies and characterized at least four structurally distinct morphologies (*3*). It was shown that above 1 mg/mL the fibrils are predominantly long and thin one-filament structures with a regular periodic pattern, while at lower concentrations the fibrils consist of two or more filaments. The molecular steps

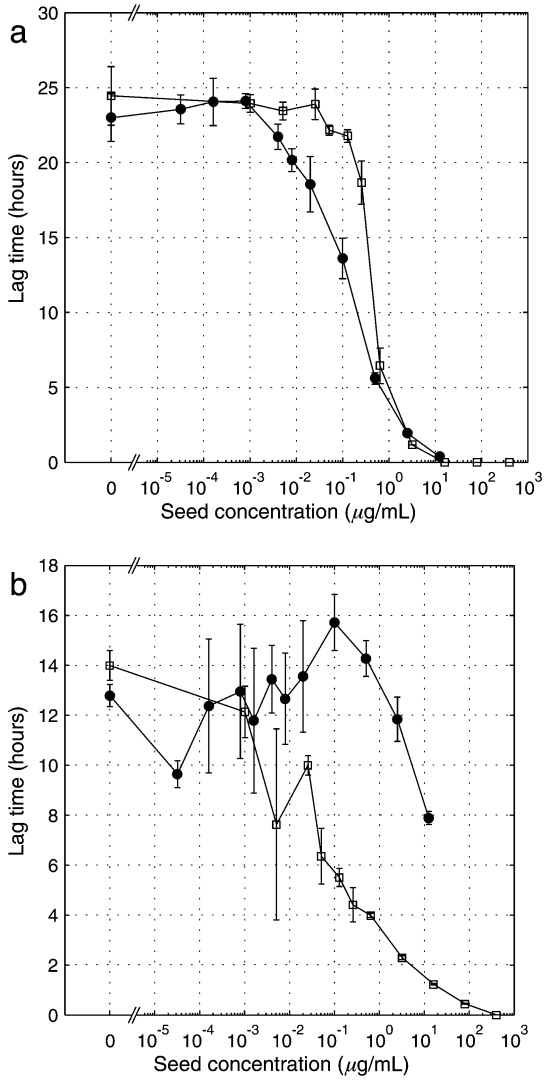

FIGURE 5: Seeding fresh glucagon solutions of 0.25 and 8 mg/mL with preformed fibrils grown at the same two concentrations under identical conditions. In each log-lin plot, the lag time of the unseeded solution is shown to the left. (a) Wells containing a fresh 0.25 mg/mL solution of glucagon. Seeding with preformed fibrils from 0.25 (●) and 8 mg/mL (□) solutions drastically reduces the lag time. (b) Wells containing an 8 mg/mL glucagon solution seeded with preformed fibrils. There is a clear reduction in lag time as the fraction of 8 mg/mL (□) fibril seeds is increased. Adding 0.25 (●) mg/mL seeds, on the other hand, is much less potent in reducing the lag time. Error bars represent the standard deviation from fibrillation at identical conditions in three separate wells.

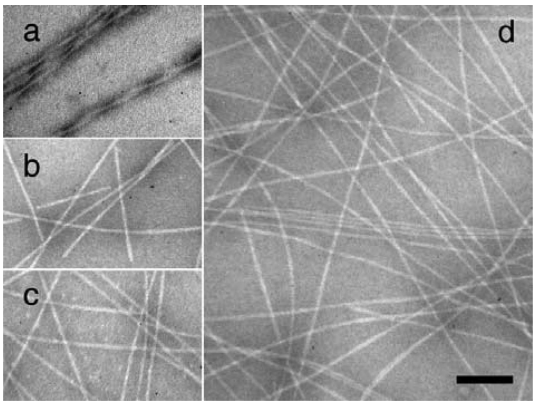

FIGURE 6: Electron microscopy pictures of fibrils from cross-seeded and self-seeded glucagon solutions. The pictures demonstrate how adding twisted seeds to a solution that normally promotes straight fibrils has no effect on fibril morphology. (a) Fresh solution of 0.25 mg/mL glucagon self-seeded with twisted fibril seeds grown in 0.25 mg/mL solution and (b) 8 mg/mL glucagon solution self-seeded with straight fibril seeds. (c) Fresh solution of 0.25 mg/mL glucagon cross-seeded with straight fibril seeds grown at 8 mg/mL and (d) 8 mg/mL glucagon solution cross-seeded with twisted fibril seeds. Maximum seed concentrations were used, i.e., 12.5 μg/mL in the case of twisted fibril seeds and 400 μg/mL in the case of straight seeds. The scale bar represents 100 nm.

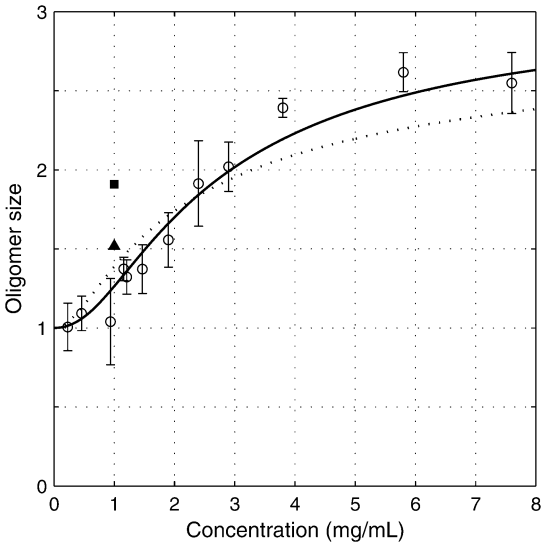

FIGURE 7: Oligomer size of fresh glucagon solutions determined by light scattering. The data show the formation of trimers at high concentrations of glucagon. The data point at 0.16 mg/mL was used for calibrating the molecular weight by assigning it an oligomer size of 1 (see Materials and Methods for details). The solid and dotted lines are fits based on the model described in the Appendix. Solid symbols show the oligomer sizes measured at 1 mg/mL with spiking of (■) 1 mM Na_2SO_4 or (▲) 45 mM NaCl.

turning a soluble protein into fibrils have been studied intensively over the years (*16*), but the reason why some morphologies are dominant under a given set of conditions and almost completely absent under slightly different conditions is still poorly understood. Our results demonstrate the existence of morphology-dependent growth inhibition. We argue that the glucagon trimer is able to influence the population of fibril morphologies present in glucagon solutions by specific inhibition of a particular fibril morphology.

Change in Kinetics Correlates with Change in Morphology. The fibrillation curves (Figure 1) all show a prolonged lag phase where apparently no fibrillation occurs. Although it is in general difficult to accurately predict the concentration dependence of lag times, the maximum lag time we observe at 1.5 mg/mL glucagon is unexpected (Figure 2). Intuitively, reducing the concentration of monomers from 1 to 0.25 mg/mL reduces the chance of monomers to come into contact and form a fibril, and we should thus expect to see an *increase* in the lag time and not, as observed, a *decrease* in the lag time (*17*). The pronounced minimum in growth rate at 1.5 mg/mL expresses the same phenomenon even more clearly. This anomalous concentration dependence is observed to correlate with a change in fibril morphology. Straight, one-filament fibrils dominate at high concentration, and regularly twisted fibrils consisting of two or more filaments dominate at low concentration.

Growth of Twisted Fibrils Is Specifically Inhibited in the Presence of Glucagon Trimers. To further characterize the

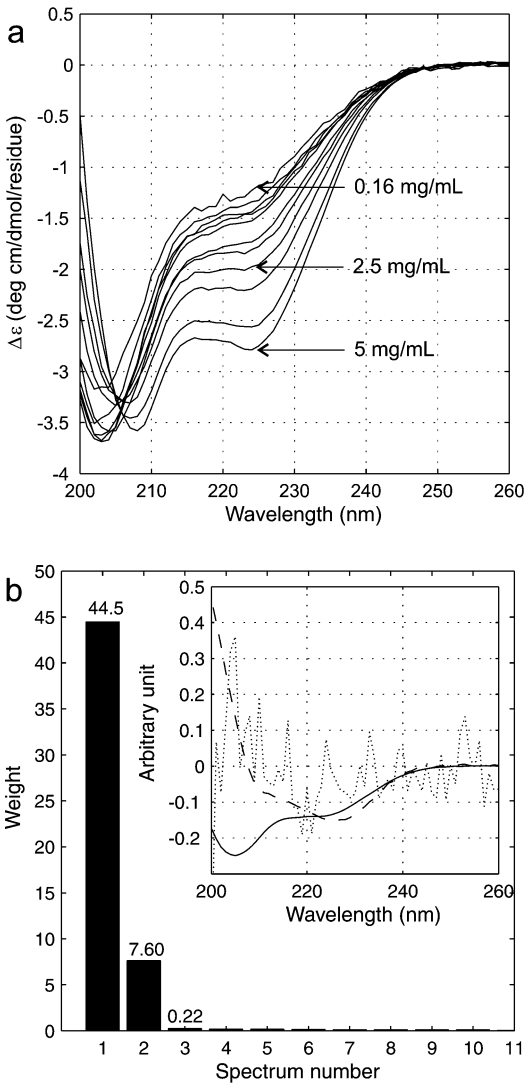

FIGURE 8: SVD of CD spectra of fresh solutions of glucagon. (a) CD spectra of fresh glucagon solutions with concentrations from 0.16 to 5 mg/mL. As the concentration is increased, the minimum at 204 nm is shifted toward 208 nm and a minimum around 224 nm appears. (b) Singular values of the decomposed basis spectra. The first two spectra have singular values of 44.5 and 7.60, respectively, while the third singular value is only 0.22. The inset shows the first three basis spectra. Two of the basis spectra (solid and dashed line) show features recognized in the raw CD spectra, and the third basis spectrum (dotted line) is very noisy.

differences between the two fibril morphologies formed from glucagon in 50 mM glycine/HCl buffer, seeding experiments were performed. In a seeding experiment, mature fibrils are disrupted into smaller fragments, seeds, by either sonication or mechanical fragmentation (*18*, *19*). In self-seeding experiments, the seeds are added to a fresh solution of the same peptide, and under the exact same buffer conditions, which the seeds originate from. This gives information about the kinetics of adding monomers to the fibril ends (*20*). Cross-seeding, on the other hand, designates an experiment where seeds are added to a solution which favors a different morphology. This includes solutions of the protein under different experimental conditions (*21*), mutants of the seed protein (*19*, *22*, *23*), and even completely different proteins (*24*−*26*). Although it is possible that the seeding effect is caused by nucleus formation on the surface of the seeds, consensus in the literature seems to be that it is caused by the addition of monomers to the ends of the seeds (*19*, *20*, *27*−*29*). In seeding experiments where a substantial decrease in lag time is observed upon seeding, the fibrils formed may either inherit the morphology of the seeds (*24*, *25*, *27*, *29*−*31*) or acquire the morphology expected from the protein solution (*23*, *32*). As an example, Yagi et al. (*28*) showed that seeding α-synuclein with seeds of hen lysozyme, *Escherichia coli* chaperonin GroES, and bovine insulin all gave a clear reduction in lag time and that in each case the original seeds were incorporated into the resulting α-synuclein fibrils (*28*, *30*). Even though the morphology of the seeded fibrils was completely different from the morphology of the original seed, the nature of the seeding effect was the addition of monomers to the seed ends.

The distinct difference between the glucagon fibril populations at low and high concentration makes glucagon fibrils very suitable for seeding experiments. The seeding experiments show (Figure 5a) that when adding seeds of either twisted or straight fibrils into a fresh solution of 0.25 mg/mL glucagon, the lag times are reduced as the seed concentration is increased above 0.1 μg/mL. In both cases the morphology is inherited from the seeds as confirmed by TEM (Figure 6a,c). Adding seeds of straight fibrils to a solution of fresh 8 mg/mL glucagon solution gave a similar reduction in lag times (Figure 5b, open squares) and the expected straight morphology (Figure 6b). Seeds of twisted fibrils, however, only had an effect at the highest concentration of 12.5 μg/mL (Figure 5b, filled circles). We believe that the small reduction in lag time at this concentration is in fact due to seeds from the small number of straight fibrils present at low concentration, since the fibrils formed are all straight (Figure 6d). The weak seed effect, if any, from twisted fibril seeds at 8 mg/mL is remarkable because the concentration of monomers in 8 mg/mL solutions is higher than in 0.25 mg/mL solutions (see below), and there should therefore be plenty of monomers from which the seeds can grow. We conclude that growth of the twisted fibrils is specifically inhibited at high concentrations.

Fibril Morphology Change Correlates with Trimer Formation. In dilute, aqueous solutions, the glucagon monomer exists as a flexible random coil structure with a small fraction (10−15%) of secondary structure at the C-terminus (*33*, *34*). In the two known crystal structures of glucagon (*34*, *35*), on the other hand, the peptide is α-helical between residue 6−26 and residue 16−26, respectively. In both crystal structures, glucagon forms a trimer. Glucagon also self-associates to form trimers in concentrated solutions at both acidic (pH 2−4.5) and alkaline (pH 9−11) conditions (*34*, *36*). The self-association is accompanied by a change in secondary structure, and approximately 35% of the molecule is α-helical in concentrated solutions (*34*, *37*). We note that the high concentration CD spectrum shows the local minima around 208 and 222 nm characteristic of α-helical-rich peptides as expected (*37*−*39*). Our static light scattering experiments confirm that glucagon self-associates in solutions at pH 2.5 buffered by a glycine/HCl buffer and that the oligomer formed has a molecular weight approximately corresponding to a trimer (Figure 7). SVD of the CD spectra measured at various concentrations determines how many components are necessary to create a linear superposition that fits the experimental spectra. Two components are sufficient (Figure 8b). This is in line with previous cross-binding experiments

(*13*) which have showed that no oligomer state other than the trimer (e.g., dimer or hexamer) is significantly populated. The appearance of straight fibrils with increasing glucagon concentration is seen to coincide with the formation of trimers.

The oligomerization data have a pronounced sigmoid shape, which is also found in other self-association studies of glucagon (*36*, *40*). The formation of trimers from monomers can be described as a reversible third-order reaction as detailed in the Appendix. Calculation of the average oligomer size as a function of total concentration according to these equations gives the dotted line in Figure 7 as the best fit to the data. This curve is clearly less sigmoid than our data. The deviation could be caused by the presence in the glucagon dry powder of ions capable of stabilizing the trimer. If present, such ions would be diluted proportionally to the dilution of glucagon, giving a more complicated equilibrium. We have tried to eliminate such ions by gel filtration. The resulting glucagon solutions showed similar oligomer sizes as before gel filtration but with larger variations between experiments (not shown). Possibly, the ions bind too tightly to be removed in this way. In general, we find that handling of dissolved glucagon should be minimized to avoid premature fibrillation. We do not know precisely which ions are present, if any, but we chose to study the effect of spiking sulfate and chloride ions into 1 mg/mL glucagon solutions. The effect of adding 1 mM Na_2SO_4 and 45 mM NaCl, respectively, is shown in Figure 7. In particular, sulfate ions are seen to stabilize oligomers, with a weaker effect from chloride ions.

We go through the calculation of a monomer−trimer equilibrium with a salt-binding trimer in the Appendix. A fit to the result is shown as a full line in Figure 7 and is seen to match the data better. With the presence of such salt ions, the monomer concentration will at highest total glucagon concentrations drop below its maximum value. The light scattering data can in fact accommodate a range of parameters (see the Appendix for details), but throughout this range the calculated monomer concentration at 8 mg/mL remains well above the concentration at 0.25 mg/mL. Hence, the fact that twisted fibril seeds grow much slower at 8 mg/mL than at 0.25 mg/mL is not due to a lower monomer concentration. Rather, on the basis of the observation that the monomer−trimer transition occurs at about the same concentration as the change in preferred morphology, we propose that the trimer can inhibit the growth of the twisted fibrils.

In the Appendix, we develop a theory of fibrillation in two distinct morphologies, with trimers inhibiting the growth of one morphology. The fits of this model to our data are shown in Figure 2. The agreement is seen to be reasonable, showing that such a model can account for the unusual concentration dependence in our data.

Sluzky et al. (*17*) have previously observed slowing of insulin fibrillation as the concentration was increased from 0.1 to 0.6 mg/mL, an effect the authors attributed to insulin dimers and hexamers saturating the hydrophobic surfaces they had placed in the sample. Our results suggest that direct interactions between insulin oligomers and the fibrils could also play a role. Even for proteins and peptides that do not form oligomers, binding of nonfibrillating conformations of the molecule to fibrils can be a mechanism

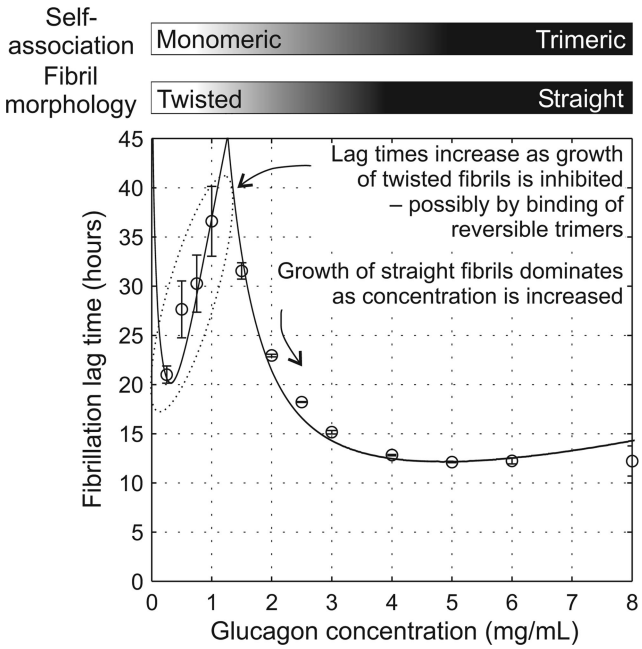

FIGURE 9: Overview of the results presented in this report. The lag times are plotted as a function of the concentration (from Figure 2). At low concentrations, glucagon is mainly monomeric, and at high concentrations, it is mainly trimeric as measured by SLS. TEM showed that the fibril morphology is twisted at low concentrations and straight at high concentrations (Figure 3).

that inhibits growth. Recently, Fink et al. (*41*) observed slowing of fibrillation of the insulin B chain when increasing the concentration from 0.2 to 0.5 μM. At higher concentrations, no fibrillation was detected, and this anomalous behavior was attributed to the formation of oligomers with increasing concentration. In the case of insulin B chain, the oligomers preferentially form protofilaments instead of mature fibrils.

ThT Binds Differently to the Two Morphologies but ThT Does Not Affect Fibrillation Kinetics. ThT dramatically increases its fluorescence quantum yield when bound to amyloid-like fibrils. The mechanism behind this property is still largely unknown, but the fluorescence yield depends among other things on pH (*42*) and on the protein forming the fibril (*43*). In the case of glucagon, Pedersen et al. (*3*) have shown that also the fibril morphology can affect the fluorescence yield. In the fibrillation kinetics at concentrations from 0.5 to 1 mg/mL (Figure 4a) one consistently observes a maximum in the ThT fluorescence intensity followed by a steady decrease in intensity. Pedersen et al. (*3*) proposed that this drop in ThT intensity is caused by a transformation from one fibril morphology to another more stable morphology (*3*). We examined the phenomenon by transferring samples from a 0.5 mg/mL solution from the plate reader directly onto a grid. This was done at maximum intensity (approximately 39 h, Figure 4b) and after 64 h where the intensity had decreased by roughly 30% (Figure 4c). As expected at this concentration of glucagon, the sample at maximum intensity showed twisted fibrils consisting of two protofibrils. The sample examined after 64 h showed a dense mesh-like net, but by diluting the sample 10-fold the close network resolved itself into twisted fibrils visually identical to the ones found after 39 h (Figure 4d).

These observations indicate that the decrease in ThT fluorescence is not related to any obvious ultrastructural

change of the individual fibrils but may reflect a different environment of ThT within the network or possibly increased light scattering artifacts due to the dense network. The fluorescence from Trp-25 is not affected by the formation of a dense network (data not shown). The same approach was applied to fibrils formed at high concentration (8 mg/mL). Even though a dense network had also formed at this concentration, no reduction in intensity is observed. Neither fibril network nor any significant decrease in fluorescence intensity was ever observed at 0.10 or 0.25 mg/mL, probably because, at these concentrations, fibril density is too low to form a network.

CONCLUSION

We have investigated glucagon fibrillation at concentrations from 0.25 to 8 mg/mL in glycine/HCl buffer at pH 2.5. The conclusions of this report are summarized schematically in Figure 9. The lag times have a maximum around 1 mg/mL. Below 0.5 mg/mL the fibrils are made up from two or more protofibrils twisting around each other with a regular twist, while above 2.5 mg/mL all fibrils consist of a single straight filament. Cross-seeding experiments show that growth of the twisted morphology is inhibited at high glucagon concentrations. This explains the increase in lag time up to 1 mg/mL, as well as the change in morphology. Glucagon is monomeric at low concentration but trimeric at high concentration. We interpret the growth inhibition as being due to trimers interacting with the twisted fibril seeds. Similar mechanisms may apply to other proteins forming polymorphic fibrils.

APPENDIX: THEORY OF TRIMERIZATION AND FIBRILLATION

In this Appendix we present a theory for the measured fibrillation lag time and rates, based on the conjecture that the increase in lag times at low glucagon concentrations is due to inhibitory binding of the glucagon trimer to the twisted morphology. The ambition is not to derive a unique model but only to demonstrate that our data are consistent with this conjecture, within a reasonable simple theory for fibrillation.

Monomer−Trimer Equilibrium. As discussed in the main text, both our data and those of previous workers indicate the existence of a monomer−trimer equilibrium for glucagon:

$$3G \rightleftharpoons G_3$$

We denote the dissociation constant by K_T: $[G]^3 = [G_3]K_T^2$. Static light scattering normalized by the average monomer mass (Figure 7) measures the average monomer size:

$$N_{av} = ([G] + 9[G_3])/[G]_{total}$$

where $[G]_{total}$ is the total amount of glucagon in the solution: $[G]_{total} = [G] + 3[G_3] = [G] + 3[G]^3/K_T^2$. It is seen that [G] as a function of $[G]_{total}$ is found as the root of a third-order polynomial. From this, the theoretical N_{av} can be calculated. The best fit to this form is shown as the dotted line in Figure 7 and is seen not to be satisfactory. As discussed in the main text, we suggest that this deviation can be due to the presence of salt ions S in our starting glucagon material. These salt ions can bind to the trimer but not to the monomer. We look at a model with three identical binding sites:

$$G_3 + 3S \rightleftharpoons G_3S + 2S \rightleftharpoons G_3S_2 \rightleftharpoons G_3S_3$$

Each ion binds independently with dissociation constant K_S: $[G_3S] = 3[G_3][S]/K_S$, $[G_3S_2] = [G_3S][S]/K_S$, $[G_3S_3] = {}^1/_3[G_3S_2][S]/K_S$, with correct accounting for binding site multiplicity. The mass balance equation now becomes

$$[G]_{total} = [G] + 3[G]^3(1 + [S]/K_S)^3/K_T^2$$

It is assumed that [S] is proportional to $[G]_{total}$, $[S] = \sigma$-$[G]_{total}$, as they are diluted together in the sample preparation. Again, [G] as a function of $[G]_{total}$ is found as the root of a third-order polynomial. Only the ratio σ/K_S enters the calculation. Our data can be fitted about equally well by a range of combinations of σ/K_S and K_T. For all combinations giving reasonable fits, the calculated monomer concentration reaches a maximum and decreases at the highest glucagon concentrations. We have chosen the parameter values to match the maximum observed in fibrillation rate constant at high concentrations, as discussed below. The resulting calculated N_{av} is shown as full lines in Figure 2.

Fibrillation Kinetics. We use a simple fibrillation model for the growth of fibril mass M and number of fibril ends N (*7*, *44*). The fibril mass grows by extension at the ends:

$$dM/dt = k_g N$$

The number of fibril ends grows by spontaneous nucleation of a rate k_{sp}. However, in order to explain the sudden growth appearing after the lag period, it is also necessary to include a secondary term proportional to the mass (*7*, *44*):

$$dN/dt = k_{sp} + k_{sec} M$$

Such a term would arise from nucleation on existing fibrils or from branching or breaking. The rates k_g, k_{sp}, and k_{sec} will depend on the monomer concentration, and possibly on the trimer concentration, and drop when the fibrillation process depletes the solution of monomers. In the present context, we are only interested in determining the lag time at a time point before the solution has been significantly depleted, so we can assume the monomer and trimer content to be constant. With the boundary conditions $M(t=0) = 0$ and $N(t=0) = 0$ the solution of $M(t)$ in this initial phase is

$$M(t) = k_{sp}(\cosh(kt) - 1)/k_{sec}$$

with $k = (k_g k_{sec})^{1/2}$. Our definition of the lag time is that the fibril mass $M(t)$ at this point reaches a particular value $M(t_{lag}) = M_{lag}$, which depends on $[G]_{total}$. This gives the relation

$$kt_{lag} = \operatorname{arccosh}(M_{lag} k_{sec}/k_g - 1)$$

Fitting Our Data to the Model. Fibril growth proceeds by the addition of monomers to fibril ends. We take this rate to be proportional to [G]. The rate of the secondary process is taken to be proportional to a power of [G] (*7*). It is our conjecture that growth of the twisted fibril morphology is inhibited by binding of the trimer, while there is no such

interaction for the straight fibrils. For the straight fibrils, then, we set

$$k_g^{\text{straight}} = k_0[\text{G}]$$

$$k_{\text{sec}}^{\text{straight}} = k_1[\text{G}]^{n_1}$$

$$k^{\text{straight}} = \sqrt{k_0 k_1}[\text{G}]^{(1+n_1)/2} = C_{\text{straight}}[\text{G}]^{n_{\text{straight}}}$$

The lag time and calculated rate constant will mainly be determined by the dominant fibril species, and we here ignore the contribution of the other morphology. On the basis of the kinetic data in Figure 2, we set the regime of the twisted fibrils to be below 1 mg/mL and that of the straight fibrils to be above 1.5 mg/mL. In Figure 2 it can be seen that the rate constant in the area dominated by straight fibrils, above 1.5 mg/mL total glucagon concentration, has a maximum between 4 and 6 mg/mL glucagon. According to the theory, this must correspond to a maximum in glucagon monomer concentration. In order for the theory to reproduce the experimental lag time maximum, we have chosen parameters for the monomer−trimer equilibrium (see above), for which the monomer concentration has its maximum in this region.

Both M_{lag} and k_{sp} will depend on the monomer concentration, and this might also be the case for the secondary process. For simplicity, we assume that the combination of these three parameters will be proportional to a power of [G]:

$$M_{\text{lag}}k_{\text{sec}}/k_{\text{sp}} = D_{\text{straight}}[\text{G}]^{m_{\text{straight}}}$$

We have simultaneously fitted the experimental values of t_{lag} and k by varying the four parameters C_{straight}, D_{straight}, n_{straight}, and m_{straight}. The latter two were poorly determined, and we have chosen to fix them at the integer values $n_{\text{straight}} = 4$ and $m_{\text{straight}} = 5$. The resulting fits are shown in Figure 2 in the region above 1.5 mg/mL.

For the twisted fibril morphology, we assume that the secondary process still is proportional to some power of the monomer concentration, while the growth process in addition to the dependence on the monomer concentration is inhibited by binding of the trimer:

$$k_g^{\text{twisted}} = k_2[\text{G}]/(1 + [\text{G}_3]/K_{\text{I}})$$

$$k_{\text{sec}} = k_3[\text{G}]^{n_3}$$

$$k^{\text{twisted}} = \sqrt{C_{\text{twisted}}(1 + [\text{G}_3]/K_{\text{I}})}[\text{G}]^{n_{\text{straight}}}$$

where K_{I} is the dissociation constant of the inhibitory trimer−fibril interaction. We expect this drop in the rate constant to account for the increase in lag time between 0.25 and 1.0 mg/mL. It can be seen in Figure 2 that the rate constant is rather poorly determined below 1 mg/mL and can accommodate many different models. For this reason, we have chosen to set the parameter combination $M_{\text{lag}}k_{\text{sec}}/k_{\text{sp}}$ to a constant D_{twisted} for the twisted fibrils. The resulting simultaneous fit to t_{lag} and k in the range 0.25−1 mg/mL is shown in Figure 2 in the region below 1.5 mg/mL.

NOTE ADDED AFTER ASAP PUBLICATION

This paper posted ASAP on May 25, 2007. Modification was made in the third equation of the Appendix and to the caption of Figure 4. The correct version reposted to the web on May 31, 2007.

REFERENCES

1. Chiti, F., Webster, P., Taddei, N., Clark, A., Stefani, M., Ramponi, G., and Dobson, C. M. (1999) Designing conditions for in vitro formation of amyloid protofilaments and fibrils, *Proc. Natl. Acad. Sci. U.S.A. 96*, 3590−3594.
2. Frokjaer, S., and Otzen, D. E. (2005) Protein drug stability: A formulation challenge, *Nat. Rev. Drug Discovery 4*, 298−306.
3. Pedersen, J. S., Dikov, D., Flink, J. L., Hjuler, H. A., Christiansen, G., and Otzen, D. E. (2006) The changing face of glucagon fibrillation: Structural polymorphism and conformational imprinting, *J. Mol. Biol. 355*, 501−523.
4. Pedersen, J. S., Flink, J. M., Dikov, D., and Otzen, D. E. (2006) Sulfates dramatically stabilize a salt-dependent type of glucagon fibrils, *Biophys. J. 90*, 4181−4194.
5. Dong, M., Hovgaard, M. B., Xu, S., Otzen, D., and Besenbacher, F. (2006) AFM Study of glucagon fibrillation via oligomeric structures resulting in interwoven fibrils, *Nanotechnology 17*.
6. Pedersen, J. S., Dikov, D., and Otzen, D. E. (2006) N- and C-terminal hydrophobic patches are involved in fibrillation of glucagon, *Biochemistry 45*, 14503−14512.
7. Ferrone, F. (1991) Analysis of protein aggregation kinetics, in *Methods Enzymol.*, 256−274.
8. Lindner, H., and Glatter, O. (2000) Determination of absolute intensity and molecular weight of small colloidal particles in the presence of some large aggregates. A combined study using static and dynamic light scattering, *Part. Part. Syst. Charact. 17*, 89−95.
9. Oberer, M., Lindner, H., Glatter, O., Kratky, C., and Keller, W. (1999) Thermodynamic properties and DNA binding of the ParD protein from the broad host-range plasmid RK2/RP4 killing system, *Biol. Chem. 380*, 1413−1420.
10. van Holde, K. E., Johnson, W. C., and Ho, P. S. (1998) *Principles of Physical Biochemistry*, Prentice Hall, Upper Saddle River, NJ.
11. Foxes Team (2006) MATRIX.xla version 2.1.
12. Stromer, T., and Serpell, L. C. (2005) Structure and morphology of the Alzheimer's amyloid fibril, *Microsc. Res. Tech. 67*, 210−217.
13. Gratzer, W. B., Creeth, J. M., and Beaven, G. H. (1972) Presence of trimers in glucagon solution, *Eur. J. Biochem. 31*, 505−509.
14. Beaven, G. H., Gratzer, W. B., and Davies, H. G. (1969) Formation and structure of gels and fibrils from glucagon, *Eur. J. Biochem. 11*, 37.
15. Glenner, G. G., Eanes, E. D., Bladen, H. A., Linke, R. P., and Termine, J. D. (1974) Beta-pleated sheet fibrils−Comparison of native amyloid with synthetic protein fibrils, *J. Histochem. Cytochem. 22*, 1141−1158.
16. Dobson, C. M. (2003) Protein folding and misfolding, *Nature 426*, 884−890.
17. Sluzky, V., Tamada, J. A., Klibanov, A. M., and Langer, R. (1991) Kinetics of insulin aggregation in aqueous solutions upon agitation in the presence of hydrophobic surfaces, *Proc. Natl. Acad. Sci. U.S.A. 88*, 9377−9381.
18. Naiki, H., Higuchi, K., Nakakuki, K., and Takeda, T. (1991) Kinetic analysis of amyloid fibril polymerization in vitro, *Lab. Invest. 65*, 104−110.
19. Jarrett, J. T., and Lansbury, P. T., Jr. (1992) Amyloid fibril formation requires a chemically discriminating nucleation event: studies of an amyloidogenic sequence from the bacterial protein OsmB, *Biochemistry 31*, 12345−12352.
20. Come, J. H., Fraser, P. E., and Lansbury, P. T., Jr. (1993) A kinetic model for amyloid formation in the prion diseases: importance of seeding, *Proc. Natl. Acad. Sci. U.S.A. 90*, 5959−5963.
21. Dzwolak, W., Smirnovas, V., Jansen, R., and Winter, R. (2004) Insulin forms amyloid in a strain-dependent manner: an FT-IR spectroscopic study, *Protein Sci. 13*, 1927−1932.
22. Morozova-Roche, L. A., Zurdo, J., Spencer, A., Noppe, W., Receveur, V., Archer, D. B., Joniau, M., and Dobson, C. M. (2000) Amyloid fibril formation and seeding by wild-type human lysozyme and its disease-related mutational variants, *J. Struct. Biol. 130*, 339−351.
23. Ramirez-Alvarado, M., and Regan, L. (2002) Does the location of a mutation determine the ability to form amyloid fibrils?, *J. Mol. Biol. 323*, 17−22.
24. Jones, E. M., and Surewicz, W. K. (2005) Fibril conformation as the basis of species- and strain-dependent seeding specificity of mammalian prion amyloids, *Cell 121*, 63−72.

25. Vanik, D. L., Surewicz, K. A., and Surewicz, W. K. (2004) Molecular basis of barriers for interspecies transmissibility of mammalian prions, *Mol. Cell 14*, 139−145.
26. Lundmark, K., Westermark, G. T., Olsen, A., and Westermark, P. (2005) Protein fibrils in nature can enhance amyloid protein A amyloidosis in mice: Cross-seeding as a disease mechanism, *Proc. Natl. Acad. Sci. U.S.A. 102*, 6098−6102.
27. Dzwolak, W., Ravindra, R., Lendermann, J., and Winter, R. (2003) Aggregation of bovine insulin probed by DSC/PPC calorimetry and FTIR spectroscopy, *Biochemistry 42*, 11347−11355.
28. Yagi, H., Kusaka, E., Hongo, K., Mizobata, T., and Kawata, Y. (2005) Amyloid fibril formation of alpha-synuclein is accelerated by preformed amyloid seeds of other proteins: implications for the mechanism of transmissible conformational diseases, *J. Biol. Chem. 280*, 38609−38616.
29. O'Nuallain, B., Williams, A. D., Westermark, P., and Wetzel, R. (2004) Seeding specificity in amyloid growth induced by heterologous fibrils, *J. Biol. Chem. 279*, 17490−17499.
30. Hong, D. P., and Fink, A. L. (2005) Independent heterologous fibrillation of insulin and its B-chain peptide, *Biochemistry 44*, 16701−16709.
31. Petkova, A. T., Leapman, R. D., Guo, Z. H., Yau, W. M., Mattson, M. P., and Tycko, R. (2005) Self-propagating, molecular-level polymorphism in Alzheimer's beta-amyloid fibrils, *Science 307*, 262−265.
32. Hasegawa, K., Yamaguchi, I., Omata, S., Gejyo, F., and Naiki, H. (1999) Interaction between A beta(1−42) and A beta(1−40) in Alzheimer's beta-amyloid fibril formation in vitro, *Biochemistry 38*, 15514−15521.
33. Gratzer, W. B., Beaven, G. H., Rattle, H. W. E., and Bradbury, E. M. (1968) A conformational study of glucagon, *Eur. J. Biochem. 3*, 276.
34. Blundell, T. L. (1983) The conformation of glucagon, in *Handbook of Experimental Pharmacology* (Lefebvre, P., Ed.) 66/I ed., pp 37−56, Springer-Verlag, Berlin.
35. Sasaki, K., Dockerill, S., Adamiak, D. A., Tickle, I. J., and Blundell, T. (1975) X-ray analysis of glucagon and its relationship to receptor-binding, *Nature 257*, 751−757.
36. Wagman, M. E., Dobson, C. M., and Karplus, M. (1980) Proton NMR-studies of the association and folding of glucagon in solution, *FEBS Lett. 119*, 265−270.
37. Srere, P. A., and Brooks, G. C. (1969) The circular dichroism of glucagon solutions, *Arch. Biochem. Biophys. 129*, 708−710.
38. Wu, C. S. C., and Yang, J. T. (1980) Helical conformation of glucagon in surfactant solutions, *Biochemistry 19*, 2117−2122.
39. Gratzer, W. B., and Beaven, G. H. (1969) Relation between conformation and association state—A study of association equilibrium of glucagon, *J. Biol. Chem. 244*, 6675.
40. Formisano, S., Johnson, M. L., and Edelhoch, H. (1977) Thermodynamics of self-association of glucagon, *Proc. Natl. Acad. Sci. U.S.A. 74*, 3340−3344.
41. Hong, D. P., Ahmad, A., and Fink, A. L. (2006) Fibrillation of human insulin A and B chains, *Biochemistry 45*, 9342−9353.
42. Khurana, R., Coleman, C., Ionescu-Zanetti, C., Carter, S. A., Krishna, V., Grover, R. K., Roy, R., and Singh, S. (2005) Mechanism of thioflavin T binding to amyloid fibrils, *J. Struct. Biol. 151*, 229−238.
43. Krebs, M. R. H., Bromley, E. H. C., and Donald, A. M. (2005) The binding of thioflavin-T to amyloid fibrils: localisation and implications, *J. Struct. Biol. 149*, 30−37.
44. Librizzi, F., and Rischel, C. (2005) The kinetic behavior of insulin fibrillation is determined by heterogeneous nucleation pathways, *Protein Sci. 14*, 3129−3134.

BI6025374